Powerful Terahertz Emission from a math xmlns="http://www.w3.org/1998/Math/MathML" display="inline" overflow="scroll">msub>mi>Bi/mi>mn>2/mn>/msub>msub>mi>Sr/mi>mn>2/mn>/msub>msub>mrow>mi>Ca/mi>mi>Cu/mi>/mrow>mn>2/mn>/msub>mrow>mrow>mi mathvariant="normal">O/mi>/mrow>/mrow>/math>$_{8+\delta}$ Mesa Operating Above 77 K

K.J. Kihlstrom, K.C. Reddy, S. Elghazoly, T.E. Sharma, A.E. Koshelev, U. Welp, Y. Hao, R. Divan, M. Tsujimoto, K. Kadowaki, W.-K. Kwok, and T.M. Benseman

Phys. Rev. Applied **19**, 034055 — Published 17 March 2023

DOI: 10.1103/PhysRevApplied.19.034055

Powerful terahertz emission from a $Bi_2Sr_2CaCu_2O_{8+\delta}$ mesa operating above 77 Kelvin

K. J. Kihlstrom[1], K. C. Reddy[1], S. Elghazoly[1], T. E. Sharma[1], A. E. Koshelev[2], U. Welp[2,*], Y. Hao[2, 3], R. Divan,[4] M. Tsujimoto[5], K. Kadowaki [6], W.-K. Kwok[2], T. M. Benseman[1,2,*]

[1] Department of Physics, Queens College of the City University of New York, 6530 Kissena Blvd., Queens NY 11367, USA

[2] Materials Science Division, Argonne National Laboratory, Lemont IL 60439, USA

[3] Department of Physics, University of Illinois at Chicago, Chicago IL 60607, USA

[4] Center for Nanoscale Materials, Argonne National Laboratory, Lemont IL 60439, USA

[5] Research Center for Emerging Computing Technologies, National Institute of Advanced Industrial Science and Technology (AIST), Ibaraki 305-8768, Japan

[6] Algae Biomass and Energy System (ABES) Research & Development Center, University of Tsukuba, Ibaraki 305-8573, Japan

[*] Authors to whom correspondence should be addressed. Email: welp@anl.gov & Timothy.Benseman@qc.cuny.edu

Abstract

Mesa-shaped structures of the high-T_c superconductor $Bi_2Sr_2CaCu_2O_{8+\delta}$ contain stacked intrinsic Josephson junctions. As such, they are a promising source of coherent radiation in the 'terahertz gap' range, spanning from approximately 0.3 THz to 2.0 THz. Technological applications of these devices become far more practical if they can be operated at a cryogenic bath temperature of 77 Kelvin or higher. Previous works have reported emission from this type of device at high THz power levels at lower operating temperatures, 40 – 60 K, while at $T_{bath} \geq$ 77 K observed power levels were generally low. Here we report generation of 130 microwatts of coherent power at 0.456 THz from a mesa of $Bi_2Sr_2CaCu_2O_{8+\delta}$ doped with 0.16 holes per Cu atom, at a bath temperature of 77.4 Kelvin. We find that the device radiates THz power when clearly-identifiable cavity modes are excited, and that the frequency and bias voltage corresponding to each of these modes is almost independent of temperature. This is consistent with these modes having THz-frequency electric fields with very little dependence on vertical position within the mesa. We also find that the THz power radiated from any given mode

decreases monotonically as the mesa temperature is increased. On the other hand, the low-frequency modes become inaccessible at low temperatures due to retrapping of the intrinsic Josephson junctions, and the maximum radiation power for the emitting mode is typically achieved at the temperature at which the retrapping voltage reaches the resonance voltage for this mode.

Introduction

Stacked 'intrinsic' Josephson junctions in the high-T_c superconductor $Bi_2Sr_2CaCu_2O_{8+\delta}$ (Bi-2212) offer the possibility of a tunable and highly compact source of continuous-wave coherent terahertz radiation, in a part of the electromagnetic spectrum which is not served well by existing technologies. Such a source would be useful for a wide range of applications in the fields of telecommunications, medical imaging, as well as in security and defense [1-4]. Operation of a mesa-shaped (Bi-2212) stack containing approximately 700 series-connected intrinsic Josephson junctions (IJJs) was demonstrated by Ozyuzer *et al.* [5] in 2007, achieving an estimated 0.5 microwatts at 0.49 THz. Subsequent development of this type of device has resulted in THz emission power levels as high as 0.61 milliwatts at 0.51 THz [6], operation temperatures as high as 86.0 Kelvin [7] and emission frequencies covering the entire frequency range from 0.3 THz up to 2.4 THz [8, 9]. In series-biased IJJ devices with a voltage bias of V_{IJJ} per junction, coherent THz emission occurs when the Josephson frequency $f_{Josephson} = 2eV_{IJJ}/h$ matches a geometric resonant mode of the mesa-shaped stack, as has been studied in detail in many previous works. (See, for instance, references [5-20] and references therein.)

In order to employ high-T_c THz sources in field-portable applications, it is highly desirable for them to be able to operate at cryogenic bath temperatures of 77.4 Kelvin or more, while still

generating technologically useful amounts of coherent THz power. This would permit the Bi-2212 stacks to be cooled by liquid nitrogen boiling at atmospheric pressure, or by very compact Stirling-cycle micro-cryocoolers using helium gas as the working fluid [21]. $Bi_2Sr_2CaCu_2O_{8+\delta}$ doped 'optimally' with $p = 0.16$ holes per Cu atom has a maximum possible T_c of around 95 Kelvin, depending on cation stoichiometry [22, 23]. Nonetheless, achieving high THz emission power at bath temperatures exceeding 77.4 K is far from trivial. Previous works report emission power levels of the order a few microwatts at these temperatures [7, 14, 24-27]. By comparison, it is generally estimated that approximately 1 milliwatt of time-averaged THz power is needed for real-time imaging applications [1, 2]. Here we demonstrate that through careful design of the geometry of the Bi-2212 stack and the chip on which it stands, it is possible to achieve 130 microwatts of coherent THz power at a bath temperature of 77.4 Kelvin, which represents a significant step towards this goal. (The total emitted THz power levels reported in this work are calculated when integrated over 2π steradians, taking measured angle-dependence of the power density into account.) A general three-dimensional overview of one of the mesas and sketch of its vertical cross section are illustrated in Figure 1a and 1b, respectively, while an optical micrograph of the THz sources we employed in this work is shown in Figure 1c.

The frequencies of the geometric resonances of the stack are determined by the in-plane mode velocity c_n , which depends on the vertical periodicity of the mode, and the boundary conditions at the top and bottom. Following the notation of reference [14], a junction stack with thickness t that contains a large number of junctions ($N = t/D \gg 1$ with D being the interlayer periodicity), and assuming boundary conditions that can be expressed as nodes or antinodes, we have a discrete set of c-axis wave vectors $k_z = n\pi/2t$ with $n = 0, 1, 2, \ldots$, giving the mode velocities [28]:

$$c_n^2 \approx \frac{c_0^2}{\varepsilon_{rc}[1 + (n\pi\lambda_{ab}/2t)^2]} \quad (1)$$

for mode indices $n \ll N/2$. Here, c_0 is the speed of light in free space, ε_{rc} is the relative out-of-plane electric permittivity, and λ_{ab} is the magnetic flux penetration depth in the direction of the CuO_2 planes. Permitted values for n depend upon the boundary conditions at the top and bottom of the mesa, as discussed in references [14] and [28]. If the stacked IJJ device has the shape of a rectangular mesa, it supports Fabry-Perot type resonances that approximately correspond to integer numbers of half-periods of the *c*-axis electric field across the width, $w = L_x$, and length, $l = L_y$, of the mesa [14, 29], such that the in-plane electromagnetic wavelengths are given as $\Lambda_{x,y} \approx 2L_{x,y}/m_{x,y}$. The frequency of the ($n$, m_x, m_y)th cavity mode is therefore:

$$f_{n,\ m_x, m_y} \approx \frac{c_n}{2}\sqrt{\left(\frac{m_x}{w}\right)^2 + \left(\frac{m_y}{l}\right)^2} \quad (2)$$

Typically, the strongest emission is seen from rectangular IJJ stacks, radiating in the (n, 1, 0) cavity mode with the smallest allowed index n.

Numerical simulations of stacked IJJs show that the probability of phase synchronization of the junctions increases with the amount of energy stored in the cavity [28]. Consequently, a higher quality factor of the collective electromagnetic excitation mode of the stack is more desirable for the purposes of enhancing THz emission power. This is given by:

$$\frac{1}{Q_{total}} = \frac{1}{Q_{JJ}} + \frac{1}{Q_{radiation}} + \frac{1}{Q_{leakage}} \quad (3)$$

At temperatures above approximately 75 Kelvin, the largest contribution to the damping $1/Q_{total}$ is from the quality factor of the Josephson oscillations themselves. At the Josephson plasma frequency ω_p , this is given by:

$$Q_{JJ} = RC\omega_p = RC\sqrt{\frac{2\pi I_c}{C\Phi_0}} \tag{4}$$

where R is the resistance of each IJJ in the stack, C is its shunt capacitance, I_c is its critical current, and Φ_0 is the flux quantum. (See W. C. Stewart, 1968 [30].) Equivalently, we can express Equation 4 in terms of the bulk c-axis properties of the extremely anisotropic BSCCO superconductor:

$$Q_{IJJ} = \rho_c n_c \sqrt{\frac{2\pi\varepsilon_0 D J_{zc}}{\Phi_0}} \tag{5}$$

where $\rho_c(T)$ is the resistive-state out-of-plane resistivity, and n_c is the far-infrared refractive index for electromagnetic waves with electric field polarized along the c-axis. ε_0 is the permittivity of free space, $J_{zc}(T)$ is the out-of-plane critical current density, and D is the junction periodicity along the c-axis. $\rho_c(T)$ can be estimated from the slope of the downward-swept branch of the mesa's (hysteretic) current-voltage characteristic, as described in [31], while $J_{zc}(T)$ can be estimated from the same datasets. The relative out-of-plane permittivity $\varepsilon_{rc} \equiv n_c^2$ is usually estimated to be about 16 for this material [32]. Using data for our Bi-2212 crystals doped with p = 0.16 obtained in reference [31] we can calculate $Q_{IJJ}(T)$. Our results are plotted in Figure 2, showing that for $T \geq 77$ K, the quality factor of the Josephson oscillations is comparatively modest, due to quasiparticle damping in the current-biased IJJs. Significant energy losses due to resistive damping of the Josephson oscillations in the mesa itself are therefore unavoidable at these bath temperatures. However, when the Q-factor of the Josephson oscillations is high, leakage of additional THz energy into the base crystal becomes relevant, whether into the Bi-2212 base crystal material directly below the mesa, or around its perimeter. In principle, these losses can be minimized by reducing the thickness of the base crystal, and/or by reducing the perimeter-to-area ratio of the mesa, thus reducing the ratio of the volume of Bi-2212 into which THz power leakage occurs to the amount of energy stored

in the resonant mode of the stack. The present work will explore these approaches as a strategy for improving THz emission power for $T \geq 77.4$ K.

Experiment

High-quality Bi-2212 single crystals were grown using the traveling solvent floating zone method. These were annealed in flowing zero-grade air at 600 °C to achieve optimal oxygen doping (p = 0.16 holes per Cu atom), and quenched by tipping them into liquid nitrogen, resulting in a superconducting T_c of 86.5 K. The crystals (typically cut to dimensions of approximately $2 \times 2 \times 0.02$ mm^3) were then mounted on $10 \times 10 \times 0.5$ mm^3 copper substrates using a metal adhesion coating and tin-lead solder. After the Bi-2212 crystal was cleaved to expose a fresh and planar surface, mesa-shaped terahertz sources were fabricated using optical lithography (using a direct-write laser pattern generator) and argon-ion etching. The widths of the mesas studied in this experiment varied as will be described below, but all mesas were 300 μm long, and 924 nm high, containing close to 596 IJJs.

During the mesa fabrication process, the crystal thickness was controlled such that the base crystal on which the resulting devices stood was only approximately 100 nm thick. This combination of minimal base crystal thickness plus a highly thermally conductive mounting arrangement is essential to ensure the highest possible thermal conductance between the base of the electrically biased IJJ stack and the cryogenic bath. Since the stack is approximately nine times thicker than the base crystal, the thermal resistance between the devices studied in this work and the cryogenic bath is dominated by the thermal resistance of the stack itself. At the bath temperatures of interest, the thermal conductivity of Bi-2212 along the crystalline c-axis (κ_c) is approximately 0.3 W.m^{-1}.K^{-1} [33]. For the $300 \times 180 \times 0.92$ μm^3 device studied here,

this implies a thermal conductance between the base plane of the mesa and the thermal bath of approximately 0.162 W/K, since the thermal resistance of the metal adhesion layer, the solder, and the copper substrate can all be neglected. The epoxies that have been used to mount Bi-2212 crystals on to substrates in THz generation experiments typically have a thermal conductivity of around 0.12 $W.m^{-1}.K^{-1}$ at typical mesa operation temperatures [34, 35], while the layer of epoxy between the substrate and the bottom of the Bi-2212 single crystal is usually of the order of 20 microns thick [34]. As a result, in most THz experiments employing epoxy-mounted Bi-2212 crystals, the thermal conductance from the device to the cryogenic bath is typically much lower than in the present work. One alternative approach to thermal anchoring developed recently by Tsujimoto *et al.* [36] is to mount the mesa on a sapphire substrate (which is both highly thermally conductive and transparent to THz radiation) using an unfilled epoxy such as Stycast 1266. The entire mesa is then encapsulated in a filled – but electrically insulating – epoxy with significant thermal conductance, such as Stycast 2850. This configuration allows the mesa to be heatsunk from the top and the sidewalls, as well as via the substrate, in addition to protecting the mesa from contaminants such as water vapor. However, the resulting thermal conductance to the bath is nonetheless much lower than in the present work, since the thermal conductance of Stycast 2850 – even at room temperature – is about 1.36 $W.m^{-1}.K^{-1}$ [37], as compared with 50 $W.m^{-1}.K^{-1}$ for the 63% Sn, 37% Pb, solder employed here [38]. At cryogenic temperatures, the difference in thermal conductivity between the two materials is likely to be even greater. Another important consequence of a thin base crystal is modification of the effective height t entering the mode velocity in Equation (1). Contrary to the standard situation of a very thick base crystal, where the parameter t is equal to the mesa height, we believe that in our case this effective height is given by the distance between the mesa top and the bottom of the crystal.

Three types of device were constructed on the same crystal: two mesas with dimensions 300 × 60 × 0.92 μm^3 designed to operate in the (n, 1, 0) mode; a mesa with dimensions 300 × 180 × 0.92 μm^3 designed to operate in the (n, 3, 0) mode; and a device consisting of an array of three conjoined mesas, each of dimensions 300 × 60 × 0.92 μm^3 and with 60 μm spacing between nearest neighbors. This latter device was intended to achieve enhanced emission power by acting effectively as three 300 × 60 × 0.92 μm^3 stacks, each operating in its (n, 1, 0) mode and electromagnetically coupled together. (See Figure 1c.) All four devices were designed to emit in the frequency range from approximately 0.4 to 0.7 THz, while operating at a range of bath temperatures from 70 K and above. For efficient THz radiation coupling to free space, it is preferable for the vertically-oriented electric fields at opposite edges of the mesa to oscillate in antiphase with respect to each other, meaning that the width of the device (or of its synchronized emitting parts) must ideally be an odd number of half-wavelengths in Bi-2212. For instance, making the width of the mesa an even number of half-wavelengths (such as by making its dimensions 300 × 120 × 0.92 μm^3) would be expected to be comparatively inefficient at emitting THz radiation with a half-wavelength of 60 μm in Bi-2212. (See reference [14].)

Devices were mounted in a closed-cycle cryostat with high-density polyethylene optical windows, while the emitted THz power was monitored using a calibrated bolometer employing a niobium transition-edge sensor in closed-loop power feedback mode, supplied by QMC Instruments Limited. The THz beam was chopped at 233.3 Hz, and the detector signal was measured using a lock-in amplifier. The power responsivity of the bolometer was determined at 0.599 THz by comparing its response with that of a calibrated pyroelectric detector employing identical THz collection geometry. The QMC bolometer collected THz radiation using a circular Winston cone with diameter of 5 mm, resulting in a collection angle of

2.18×10^{-4} steradians in our measurement configuration. It was found to have an optical THz responsivity of 9350 V/W (before signal preamplification) for radiation incident upon the bolometer's (circular) outer window that falls within the field of view of its collection optics, independent of THz polarization orientation. We also measured THz emission power levels from the devices studied in this work using a liquid helium-cooled silicon bolometer supplied by Infrared Laboratories, also employing a circular Winston cone. This bolometer was also calibrated in the same manner using the same pyroelectric detector, and the implied THz power levels were found to agree within uncertainties (of approximately +/- 5%) when measured with either of these bolometer systems. These power level uncertainties were primarily limited by small uncertainties associated with the precise dimensions and alignment of the THz collection geometries. The Infrared Laboratories bolometer was found to have an optical THz responsivity of 4970 V/W (before signal preamplification) for radiation incident upon the bolometer's outer window that falls within the field of view of its collection optics. Further details of our calibration procedures can be found in the Supplemental Material of reference [6].

The mesas were current-biased, with the soldered connection between the base crystal and the copper substrate acting as a return current lead. The voltage across the current-driven mesa was measured by using an adjacent unbiased mesa as a negative voltage tap. (Due to the extreme anisotropy of Bi-2212, this mesa is effectively at the same potential as the base of the driven mesa.) At each bath temperature studied, the bias current was swept up until all of the IJJs were driven into the resistive state, and then swept back down continuously at 40 μA per second to measure the bias-dependence of the THz emission.

An example of such a current-voltage sweep for the 300 × 180 × 0.92 μm^3 mesa at a bath temperature of 77.4 Kelvin (just above the boiling point of liquid nitrogen at sea level) is plotted

in Figure 3a, together with the voltage-dependence of the emitted THz power. The angle-dependence of the emitted THz radiation was measured for the devices studied in this work, and was found to be very similar to that reported by Minami *et al.* [39]. Power levels plotted in Figures 3, 4, 5, and 7 were obtained by normalizing the power level measured at $(\theta = 45°,\ \phi = 0°)$ to 2π steradians, incorporating an appropriate angle-dependence. (See Figure 6.) Figures 3b and 3c respectively show details of the THz emission and I-V characteristics in the region in which the mesa emits maximum THz radiation at 77.4 K. The dashed black line in Figure 3c is a straight line fitted through the origin, allowing us to estimate the current drawn by the mesa in the absence of THz resonance modes. (We note that in the absence of energy loss to any geometric or bosonic resonant modes, the current-voltage characteristics are weakly nonlinear with only small upward curvature, $d^2I(V)/dV^2 \geq 0$, meaning that we can estimate the small-bias resistance of the mesa by identifying a straight line through the origin which is the tangent to $I(V)$.) As was done in reference [28], we may then estimate the excess current drawn by the mesa due to THz resonances being excited, and thus the power delivered to the THz mode. At peak emission intensity at 77.4 K, we estimate 6.8 mA of excess current, and 4.0 mW of excess power. Since we measure 130 μW of emitted THz power under these conditions, this implies that approximately 3.3% of the power delivered to the THz mode is being converted to far-field radiation. Since the base crystal in this experiment is only 100 nm thick and the temperature is quite close to T_c, it is likely that dissipation under these emission conditions is dominated by quasiparticle losses inside the mesa itself. Equivalent calculations performed in reference [28] estimated that emitted THz radiation was 2.5% of the power delivered to the cavity resonance in that experiment. However, the mesa in reference [28] stood on a Bi-2212 base crystal approximately 20 microns thick, was underdoped (T_c = 76.3 K) and was operated at 20 – 30 K, so such a level of agreement in the emission efficiency of these two devices is actually quite surprising. Similar dramatic

deviations from a linear I-V characteristic at THz emission resonances were previously reported by Kitamura *et al.* [26]. Cattaneo *et al.* have very recently reported a THz emission power efficiency of 12% of the input DC power, as obtained from a small mesa microfabricated upon a Bi-2212 whisker, emitting at 4.0 THz [40].

As the bias current is swept through the level corresponding to maximum THz emission, the mesa voltage undergoes a jump of -35 mV in total at constant current, followed by a second jump of +10 mV as the current is swept below the level associated with maximum emission. (The jumps are labelled by the arrows and red asterisks in Figures 3b and 3c). The -35 mV jump is highly reproducible, as shown in the Appendix, and does not show the current hysteresis that would be expected if it were associated with retrapping of one or more IJJs in the mesa itself, or in the base crystal immediately below it. Since this jump cannot be explained via Josephson retrapping, we therefore suggest that these features are most probably due to a discontinuous change in the power drawn by the cavity resonance while the mesa is being biased at constant current. Such voltage jumps are most probably due to sudden changes in the fraction of synchronized junctions in the stack, and were predicted by our earlier numerical Lawrence-Doniach simulations in [28]. (See for instance Figure 5 of reference [28].) The +10 mV jump occurs at a highly reproducible current (see the Appendix) but the size of the jump shows a certain amount of statistical variation, implying that the collapse of the highly synchronized state associated with this jump may not be complete, and that after the jump occurs, some of the IJJs remain synchronized and generating THz radiation.

At lower bias currents, the IJJs retrap, over a range of currents that vary by a factor of between 10% and 20%, depending upon the cryogenic bath temperature. Retrapping of Bi-2212 IJJs is a statistical process that for small-size stacks has previously been thoroughly studied and found

to agree well with theoretical expectations [41]. In larger stacks such as those studied here, retrapping is found to occur at higher current densities than expected, and the reasons for this have not been conclusively established. Once the bias current is sufficiently low for retrapping to begin, the shape of the I-V curve will be different for each realization of the measurement. Since self-heating in our devices at these bias currents is comparatively low (as we will discuss later) the per-IJJ electrical resistance changes little as a function of the number of junctions switched to the resistive state, implying that the spread of retrapping voltages is only about 10% to 20%, even as the total stack voltage varies substantially. As shown in Figures 3, 4 and 5, THz emission can occur even when only a subset of the stack is still in the resistive state. Our results show that this can be observed for as few as 200 IJJs remaining in the resistive state.

An example of a resulting THz emission spectrum measured using an FTIR spectrometer is plotted in Figure 3d, with greatest intensity at 0.456 THz. The linewidth shown in Figure 3d is limited by the 2.25 GHz resolution of our spectrometer, and the true linewidth is likely to be even narrower than this [42]. The linewidth would be determined by the quality factor in the situation when the cavity is excited by unsynchronized IJJs with a broad frequency distribution. This scenario is clearly not realized in our system, since the as-measured linewidth would imply a quality factor of at least $Q = f/\Delta f \approx 114$, which is much narrower than $Q \approx 22$ as calculated using Equation (5) for Bi-2212 doped with $p = 0.16$ at $T = 77.4$ K, as can be seen from Figure 2. This result is an experimental demonstration of the established theoretical prediction that for emission modes of stacked IJJs, the linewidth of the THz emission is determined *not* by the quality factor of the Josephson oscillations, but instead by the level of thermal noise present in the stack (which adds to the junction bias voltage provided by the power supply), plus – in some cases – the failure of all of the IJJs in the stack to phase-lock to

the same frequency 100% of the time. This phenomenon of partial synchronization was simulated and analyzed using a Lawrence-Doniach model for a nonuniform IJJs stack with a trapezoidal cross section including thermal noise, by some of the authors in [28].

Figure 4 shows the evolution of the current-voltage and THz emission characteristics for the same 300 × 180 × 0.92 μm^3 mesa, as the bath temperature is changed in 5 Kelvin steps. As usual, the increasing current drives IJJs in the mesa into dynamic resistive states until all junctions are switched and the full dynamic state is reached. This state is preserved with decreasing current until the IJJs start to switch back to static states (retrap). The retrapping current increases with decreasing temperature. The non-monotonic behavior of I-V curves at higher currents observed at temperatures below 60 K is caused by heating effects. This is usual behavior for mesas fabricated on top of Bi-2212 crystals [5-18]. The maximum voltage ranging from 1.5 V at 60 K to 4.1 V at 25 K, however, is unusually high due to the efficient heat management in our structure.

The voltage jumps seen at bias voltages in excess of 2 V for $T \leq 45$ K are not due to any kind of Josephson switching, but instead due to the hysteretic collapse of localized current filaments in the mesa, so called 'hot spots'. These filaments can occur due to the fact that for under-doped or optimally-doped Bi-2212 (i.e. for $p \leq 0.16$), $d\sigma_c/dT > 0$ for all $T \leq T_c$, which can give rise to localized thermal runaway for certain combinations of bath temperature and biasing conditions. This phenomenon was studied and analyzed in detail by Wang and Kleiner *et al.* [43, 44], and by some of the authors, in reference [45].

The high values of the maximum voltages in our device allow us to observe excitation of the higher-order modes, which are usually inaccessible. Indeed, the voltage dependences of the

radiation power at different temperature presented in Figure 4b demonstrate rich peak structure. At low temperatures, we only observe the modes with high indices yielding low radiation power, because the low-frequency modes are inaccessible due to retrapping. With increasing temperature the retrapping current decreases and the modes with lower indices become accessible, which have higher radiation power. As a consequence, the maximum achievable radiation power *increases* with decreasing temperature. Figure 5 shows the evolution of the emitted THz power with respect to bias voltage, over a range of more closely-spaced temperatures, closer to T_c. Between 60 Kelvin and 80 Kelvin, the voltage dependence of the power displays complicated structure, partly caused by hysteretic retrapping events. Nevertheless, groups of emission lines can be identified that do not shift with temperature (marked by vertical dashed lines) while the entire pattern seems to shift to lower frequencies at higher T. A temperature-independent emission frequency for any given mode clearly implies that the vertical mode index n in Equation (1) is zero for all observed excited modes. Similar behavior has been observed in stand-alone mesas in references [46] and [47].

By contrast, using experimental values for $\lambda_{ab}(T)$ for optimally-doped Bi-2212 with $p = 0.16$ measured by Anukool *et al.* [48], we would expect THz modes with $n = 1$ to drop in frequency and corresponding bias voltage by approximately 30% over this temperature range. Modes with $n > 1$ would be expected to drop in frequency even further. (See Equations 1 and 2.) Such temperature-dependent behavior has been observed in mesas fabricated on the top of large crystals [28]. We can therefore conclude that any THz modes being strongly excited in this device have $n = 0$, which is consistent with these modes having antinodes of the c-axis electric field at both the top of the mesa and the bottom of the Bi-2212 base crystal. The presence of these antinodes is in turn consistent with this mesa having a thick gold electrode on top, while standing on a 100 nm base crystal, which itself in turn stands on a thick layer of gold. Since

our base crystal is only approximately 100 nm thick, the THz modes are expected to extend from the top of the mesa to the bottom of the base crystal, with minimal variation over this height of the *c*-axis electric field strength associated with each mode that has $n = 0$. At THz frequencies, the skin depth in thermally evaporated Au thin films can be estimated to be about 20 nm, using experimental values for Au thin film sheet resistance obtained from references [49], [50], and [51]. The 150 nm Au top electrode is sufficiently thick that it substantially exceeds the gold's skin depth, so that the presence of the 500 nm Au current leads at either end of the mesa are not expected to affect the nature of the resonant modes there. This is in contrast to the situation identified for a 30 nm top electrode in reference [14].

The multiple THz emission power peaks shown in Figure 5 imply that modes with different $(n = 0,\ m_x,\ m_y)$ are being excited at different cryogenic bath temperatures. The values of the emission frequencies for the 300 × 180 × 0.92 μm^3 mesa can be interpreted assuming a far-infrared refractive index of 4.24 for optimally-doped Bi-2212 with p = 0.16, and resulting frequencies of important resonant modes of this device are listed in Table I. This interpretation suggests that the strongest emission achieved at 77.4 K is due to the $(n = 0,\ m_x = 0,\ m_y = 4)$ mode, resulting in 130 μW of total radiated power at 0.456 THz. Even though this mode has even m_y, it is likely to radiate THz power more strongly than might be naïvely expected, since the 500 nm Au current lead almost completely covers one end of the mesa, meaning that the THz radiation from the ends of the mesa would not be expected to cancel itself out in the far-field limit. Since the responsivity of our THz detector setup is independent of polarization angle, we expect that the differences observed in mode intensities are most probably due to some modes radiating more efficiently in the far-field limit than others. It is also likely that different mode indices result in different angular emission patterns, resulting in different collection efficiencies for any given choice of θ and ϕ. An important future experiment will

be to compare angular dependence of the emission for different modes. An additional important future experiment would be to collect and focus as much of the emitted THz power as possible using a photoconductive antenna as was performed by An *et al.* [52], allowing a more direct comparison for the THz power emitted by different modes.

At lower bath temperatures, emission is also seen from higher frequency modes. The strongest of these is observed most clearly at 70 K, and is most likely to be the $(n = 0,\ m_x = 3,\ m_y = 0)$ mode, which is approximately degenerate with the $(n = 0,\ m_x = 0,\ m_y = 5)$ mode, due to the dimensions of this device. THz emission from these two degenerate modes is found to consistently result in broad, multipeaked spectra. It is likely that the near-degeneracy of these two modes results in unstable synchronization characteristics of the IJJs, suggesting that this is a characteristic that should be avoided if narrow emission linewidth is desirable, as is usually the case. Figure 6 shows the emission spectrum from this mode, together with the angle dependence of its emission intensity. A relevant future experiment will be to study the emission modes from this device with much higher frequency resolution using heterodyne mixing techniques, as was performed in References [39] and [42].

A further strong emission peak seen at approximately 0.84 V over a wide range of temperatures (see Figure 5) is most likely to correspond to the $(n = 0,\ m_x = 3,\ m_y = 3)$ mode, while a broad THz emission peak at approximately 1.00 V is likely to correspond to the $(n = 0,\ m_x = 4,\ m_y = 0)$ mode. At voltages above 1.00 V, emission is seen over a broad range of voltages, which is likely to be the result of a large number of modes whose different values of $(n = 0,\ m_x,\ m_y)$ result in closely-spaced mode energies.

The total radiated THz power for each of the above modes of the 300 × 180 × 0.92 μm^3 mesa is plotted as a function of temperature in Figure 7a. The major limiting factor preventing excitation of low-frequency modes at low temperatures is retrapping of the IJJs when the current drops below a certain value. Decrease of the retrapping current with increasing temperature allows the excitation of modes with lower frequencies, excited at lower per-junction bias voltages. At the same time, emission from higher-frequency THz modes becomes suppressed more quickly as the bath temperature is increased. This is most probably due to higher-frequency modes requiring higher bias voltage and current, resulting in higher self-heating and consequent loss of IJJ synchronization at lower bath temperatures as compared with lower-frequency modes.

Figure 7b shows the behavior of the maximum power achievable at each bath temperature studied, for all four devices investigated. In all four cases, emitted THz power increases as temperature is increased, peaking between 70 K and 75 K. We wish to emphasize, however, that such behavior is caused by the emergence of the modes with low indices characterized by higher emission power, while the power emitted from any given mode monotonically decreases with increasing temperature, as shown in Figure 7a. Maximum emission power decreases rapidly as the bath temperature is increased above 77.0 K. The two mesas with dimensions 300 × 60 × 0.92 μm^3 show comparatively consistent emission power characteristics, while the wider mesa with dimensions 300 × 180 × 0.92 μm^3 shows significantly enhanced emission above 70 K relative to the 300 × 60 × 0.92 μm^3 mesas. Making the mesa wider is likely to have two effects. Firstly, it increases the total length of the mesa sidewalls, enhancing the THz power coupling to free space. Secondly, tripling the mesa width decreases the mesa's perimeter-to-area ratio, thus reducing the importance of energy losses into the surrounding base crystal as described above. Both of these effects are likely to improve emission performance, especially

at bath temperatures close to T_c. The greatest achievable power from this device was just over 160 microwatts, obtained at a bath temperature of 76.5 Kelvin. At bath temperatures achievable with liquid nitrogen at atmospheric pressure, (77.4 Kelvin) over 130 μW was generated from the 300 × 180 × 0.92 μm^3 mesa. At a bath temperature of 55 K, this mesa was able to emit at much higher bias voltages and emission frequencies, namely generating in excess of 40 μW at approximately 0.910 THz.

The device consisting of 3 conjoined mesas shows very similar emission intensity as a function of temperature, at the cost of having a total area footprint some 40% larger than that for the 300 × 180 × 0.92 μm^3 mesa. Since this set of conjoined mesas showed a roughly fourfold increase in maximum power output relative to the 300 × 60 × 0.92 μm^3 mesas, this implies that only two out of the three conjoined mesas were effectively synchronizing, and that the third mesa was not significantly contributing to the THz emission power. All of the mesas studied showed back-bending of their I-V curves at sufficiently high current bias. However, due to the very strong heatsinking in these devices, the bias voltages at which this occurred were always much larger than the Josephson voltage for any resonant mode that could be efficiently excited. Consequently, no THz emission was detected in the back-bending regime, in contrast to what is commonly observed for Bi-2212 mesas whose base crystals are mounted on epoxy.

Discussion and Conclusions

By constructing $Bi_2Sr_2CaCu_2O_{8+\delta}$ mesas doped with $p = 0.16$, and with greatly enhanced heat sinking allowing us to design larger devices with a correspondingly lower perimeter-to-area ratio, we have obtained 130 μW of coherent, continuous-wave radiation at 0.456 THz, and a cryogenic bath temperature of 77.4 K. This represents an improvement of over an order of magnitude beyond previously reported results for this type of device operating at $T_{bath} \geq 77$ K,

as reported in references [7], [14], [17 – 20], and [24]. At 76.5 K, just below the boiling point of liquid nitrogen, the same device emitted over 160 μW. We attribute these advances to the fact that our samples are far more strongly heatsunk than those previously reported. This was achieved by using a copper substrate instead of sapphire, and mounted using tin-lead solder instead of electrically-conductive epoxy as well as by using a very thin base Bi-2212 crystal, of approximately only 100 nm in thickness. This allows the bath temperature to be brought much closer to T_c without the mesa self-heating unacceptably close to T_c and strongly reducing the superfluid density in the device.

Previous calculations and numerical simulations by one of the authors have studied the phenomenon of THz power leakage from Bi-2212 IJJ stacks into the base crystal [53]. These studies show that for Bi-2212 with $p = 0.16$ operating at temperatures above 40 Kelvin, the base crystal becomes effectively transparent to THz radiation if it is less than approximately 1 micron thick. Consequently, THz power losses in the base crystal become negligible, and a noble metal layer underneath the base crystal will act as an effective mirror for THz radiation. For devices with very thin base crystals mounted on noble metal (such as the ones studied here), coupling of THz radiation from the IJJ stack into free space will therefore depend only upon the electromagnetic characteristics of the stack itself, and not significantly upon the lateral dimensions of the base crystal or its precise thickness. In addition to the results reported in the present work, we have also observed 40 – 50 microwatts of total emitted THz power from five other Bi-2212 mesa devices fabricated upon two other chips, both of which have base crystals that are approximately 100 nm thick and soldered to copper substrates. In all of these devices, the lateral IJJ stack dimensions were 60×300 μm^2, and stack heights ranged from 0.75 μm to 0.95 μm.

It is likely that substantial further improvements in the THz power level could be achieved by either increasing the number of stacked junctions, increasing the length of the device, or both. It is already well established that the power emitted from the stack into an un-matched load scales as the square of the number of stacked junctions oscillating in phase [5]. Theoretical considerations predict that the emitted THz power in the (n, 1, 0) mode scales as roughly L_y^2 when L_y is less than the wavelength in free space of the emitted THz radiation (approximately 600 microns for the devices studied here), and as L_y thereafter [54].

For a mesa with only modest self-heating, and which is strongly heatsunk at its base to the cryogenic bath, the power dissipation density within the mesa can be approximated as uniform, allowing the heat diffusion equation to be approximately solved analytically. In this limit, the temperature within the mesa as a function of height z above the base of the mesa is given by the following equation:

$$T(z) = \frac{P}{\kappa_c}\left(tz - \frac{z^2}{2}\right) + \frac{Pwlt}{G} + T_{bath} \tag{6}$$

where P is the DC power density inside the mesa, κ_c is the c-axis thermal conductivity, w and l are the mesa's width and length, t is its c-axis thickness, and G is the thermal conductance connecting the base of the mesa to the bath. When the 300 × 180 × 0.92 μm^3 device is operating at its peak THz power output (at 0.456 THz) for $T_{bath} = 77.4$ K, it dissipates approximately 39 mW. Equation 6 predicts that under such conditions, the bottom of the mesa ($z = 0$) self-heats to 78.0 K, and the top of the mesa ($z = t$) self-heats to 78.7 K. If the thickness of the device were increased to 1.3 μm, it would increase the temperature at the top of the mesa only to 79.4 K (under equivalent biasing conditions, such that the voltage per IJJ is kept the same). While it is perhaps premature to speculate, one might therefore envisage a mesa of dimensions

$1000 \times 180 \times 1.3$ μm^3, which might be expected to generate approximately 2.0 mW of THz power at roughly 0.456 THz.

By employing a crystal with a T_c of 91.5 K, Sun *et al*. were able to generate approximately 100 nW of radiated THz power at $T_{bath} = 86.0$ K [7]. These results suggest that the same THz power output levels from the type of device demonstrated in the present work could be achieved at still higher temperatures by using a $Bi_2Sr_2CaCu_2O_{8+\delta}$ crystal with different Bi:Sr stoichiometry and therefore a higher T_c^{max} than 86.5 K (as was employed here) thus increasing the amount of available thermal headroom.

Acknowledgements

Work at Argonne National Laboratory was funded by the US Department of Energy, Office of Science, Basic Energy Sciences, Materials Sciences and Engineering Division. Patterning of the Bi-2212 mesas was performed at Argonne's Center for Nanoscale Materials (CNM). Use of the Center for Nanoscale Materials, an Office of Science user facility, was supported by the U.S. Department of Energy, Office of Science, Office of Basic Energy Sciences, under Contract No. DE-AC02-06CH11357. This work was also supported by the National Science Foundation under Grant No. 2045957. We would also like to acknowledge funding from PSC-CUNY grants TRADB-47-573 and TRADB-48-476, and from the Japanese Society for the Promotion of Science under Grant No. 19H02540.

Appendix

Figure 8 illustrates the reproducibility of the phenomena plotted in Figure 3. Figure 8a shows the reproducibility of the voltage jumps that we provisionally attribute to the formation and collapse of a synchronized state in the 300 × 180 × 0.92 μm^3 mesa at a cryogenic bath temperature of 77.4 K. In Figure 8a, we plot current-voltage measurements recorded while sweeping the current downwards or upwards through these jumps. Ten sets of data are plotted sweeping in each direction. The -35 mV jump (as defined when sweeping the current downwards) that occurs at a bias current of around 65.7 mA is highly reproducible in size, occurs over a range of +/- 100 μA, and shows very little hysteresis compared to the jumps associated with Josephson switching in this device. The +10 mV jump occurring at a bias current of around 63.5 mA occurs at a highly reproducible current, but the size of the voltage increase shows some variation from one measurement to the next, and this voltage increase is hysteretic – in other words, it cannot be reversed without sweeping the bias current above 66 mA again. (For clarity, these upsweep curves are not shown in the plot.) This behavior was predicted by our numerical simulations performed in reference [28]. Since Josephson retrapping cannot account for a *positive* voltage jump, we provisionally attribute this +10 mV jump to the partial collapse of the synchronized state. Collapse of this state may not be complete, as THz emission is still detected at bias currents immediately below this voltage jump.

Figures 8b and 8c show the excellent reproducibility of the THz emission power behavior for the same range of voltages and bias currents. Five datasets are plotted, all collected for continuous downward current sweeps. There is some variation between datasets when plotted as a function of voltage, due to the voltage jumps occuring at slightly different currents for

each realization of the measurement. However, there is almost no discernable variation between these datasets when the data is plotted as a function of bias current.

References

[1] Special issue "T-ray imaging, sensing, & detection" Proceedings of the IEEE **95**, nr. 8 (2007).

[2] M. Tonouchi, "Cutting-edge terahertz technology", Nature Photonics **1**, 97 (2007).

[3] S. S. Dhillon, M. S. Vitiello, E. H. Linfield, A. G. Davies, M. C. Hoffmann, J. Booske, C. Paoloni, M. Gensch, P. Weightman, G. P. Williams, E. Castro-Camus, D. R. S. Cumming, F. Simoens, I. Escorcia-Carranza, J. Grant, S. Lucyszyn, M. Kuwata-Gonokami, K. Konishi, M. Koch, C. A. Schmuttenmaer, T. L. Cocker, R. Huber, A. G. Markelz, Z. D. Taylor, V. P. Wallace, J. A. Zeitler, J. Sibik, T. M. Korter, B. Ellison, S. Rea, P. Goldsmith, K. B. Cooper, R. Appleby, D. Pardo, P. G. Huggard, V. Krozer, H. Shams, M. Fice, C. Renaud, A. Seeds, A. Stöhr, M. Naftaly, N. Ridler, R. Clarke, J. E. Cunningham, and M. B. Johnston, The 2017 terahertz science and technology roadmap, J. Phys. D: Appl. Phys. **50**, 043001 (2017).

[4] G. Valusis, A. Lisauskas, H. Yuan, W. Knap, and H. G. Roskos, Roadmap of Terahertz Imaging 2021, Sensors **21**, 4092 (2021).

[5] L. Ozyuzer, A. E. Koshelev, C. Kurter, N. Gopalsami, Q. Li, M. Tachiki, K. Kadowaki, T. Yamamoto, H. Minami, H. Yamaguchi, T. Tachiki, K. E. Gray, W.-K. Kwok, and U. Welp, Emission of coherent THz radiation from superconductors, Science **318**, 1291 (2007).

[6] T. M. Benseman, K. E. Gray, A. E. Koshelev, W.-K. Kwok, U. Welp, H. Minami, K. Kadowaki, and T. Yamamoto, Powerful terahertz emission from $Bi_2Sr_2CaCu_2O_{8+\delta}$ mesa arrays, Appl. Phys. Lett. **103**, 022602 (2013).

[7] H. Sun, R. Wieland, Z. Xu, Z. Qi, Y. Lu, Y. Huang, H. Zhang, X. Zhou, J. Li, Y. Wang, F. Rudau, J. S. Hampp, D. Koelle, S. Ishida, H. Eisaki, Y. Yoshida, B. Jin, V. P. Koshelets, R. Kleiner, H. Wang, and P. Wu, Compact High-T_c Superconducting Terahertz emitter operating up to 86 K, Phys. Rev. Applied **10**, 024041 (2018).

[8] T. Kashiwagi, T. Yamamoto, T. Kitamura, K. Asanuma, C. Watanabe, K. Nakade, T. Yasui, Y. Saiwai, Y. Shibano, H. Kubo, K. Sakamoto, T. Katsuragawa, M. Tsujimoto, K. Delfanazari, R. Yoshizaki, H. Minami, R. A. Klemm, and K. Kadowaki, Generation of electromagnetic waves from 0.3 to 1.6 terahertz with a high-T_c superconducting $Bi_2Sr_2CaCu_2O_{8+\delta}$ intrinsic Josephson junction emitter, Appl. Phys. Lett. **106**, 092601 (2015).

[9] T. Kashiwagi, K. Sakamoto, H. Kubo, Y. Shibano, T. Enomoto, T. Kitamura, K. Asanuma, T. Yasui, C. Watanabe, K. Nakade, Y. Saiwai, T. Katsuragawa, M. Tsujimoto, R. Yoshizaki, T. Yamamoto, H. Minami, R. A. Klemm, and K. Kadowaki, A high-T_c intrinsic Josephson junction emitter tunable from 0.5 to 2.4 terahertz, Appl. Phys. Lett. **107**, 082601 (2015).

[10] T. Kashiwagi, M. Tsujimoto, T. Yamamoto, H. Minami, K. Yamaki, K. Delfanazari, K. Deguchi, N. Orita, T. Koike, R. Nakayama, T. Kitamura, M. Sawamura, S. Hagino, K. Ishida, K. Ivanovic, H. Asai, M. Tachiki, R. A. Klemm, and K. Kadowaki., High Temperature Superconductor Terahertz Emitters: Fundamental Physics and Its Applications, Japanese Journal of Applied Physics **51**, 010113 (2012).

[11] T. Tachiki, H. Katada, and T. Uchida, Evaluation of Cavity Modes in Superconducting Intrinsic-Josephson-Junction Oscillators for Terahertz-wave Generation, Journal of Infrared Millimeter and Terahertz Waves **35**, 509–516 (2014).

[12] A. Elarabi, Y. Yoshioka, M. Tsujimoto, and I. Kakeya, Monolithic Superconducting Emitter of Tunable Circularly Polarized Terahertz Radiation, Phys. Rev. Applied **8**, 064034 (2017).

[13] A. Elarabi, Y. Yoshioka, M. Tsujimoto, and I. Kakeya, Circularly polarized terahertz radiation monolithically generated by cylindrical mesas of intrinsic Josephson junctions, Appl. Phys. Lett. **113**, 052601 (2018).

[14] T. M. Benseman, A. E. Koshelev, V. Vlasko-Vlasov, Y. Hao, U. Welp, W.-K. Kwok, B. Gross, M. Lange, D. Koelle, R. Kleiner, H. Minami, M. Tsujimoto, and K. Kadowaki,

Observation of a two-mode resonant state in a $Bi_2Sr_2CaCu_2O_{8+\delta}$ mesa device for terahertz emission, Phys. Rev. B **100**, 144503 (2019).

[15] G. Kuwano, M. Tsujimoto, Y. Kaneko, T. Imai, Y. Ono, S. Nakagawa, S. Kusunose, H. Minami, T. Kashiwagi, K. Kadowaki, Y. Simsek, U. Welp, and W.-K. Kwok, Mesa-Sidewall Effect on Coherent Terahertz Radiation via Spontaneous Synchronization of Intrinsic Josephson Junctions in $Bi_2Sr_2CaCu_2O_{8+\delta}$, Phys. Rev. Applied **13**, 014035 (2020).

[16] U. Welp, K. Kadowaki, and R. Kleiner, Superconducting emitters of THz radiation, Nature Photonics **7**, 702 (2013).

[17] I. Kakeya and H. B. Wang, Terahertz-wave emission from Bi2212 intrinsic Josephson junctions: a review on recent progress, Supercond. Sci. Technol. **29**, 073001 (2016);

[18] T. Kashiwagi, H. Kubo, K. Sakamoto, T. Yuasa, Y. Tanabe, C. Watanabe, T. Tanaka, Y. Komori, R. Ota, G. Kuwano, K. Nakamura, T. Katsuragawa, M. Tsujimoto, T. Yamamoto, R. Yoshizaki, H. Minami, K. Kadowaki, and R. A. Klemm, The present status of high-T_c superconducting terahertz emitters, Supercond. Sci. Technol. **30**, 074008 (2017).

[19] R. Kleiner and H. B. Wang, Terahertz emission from $Bi_2Sr_2CaCu_2O_{8+\delta}$ intrinsic Josephson junction stacks, J. Appl. Phys. **126**, 171101 (2019).

[20] K. Delfanazari, R. A. Klemm, H. J. Joyce, D. A. Ritchie, and K. Kadowaki, Integrated, Portable, Tunable, and Coherent Terahertz Sources and Sensitive Detectors Based on Layered Superconductors, Proceedings of the IEEE **108**, 721 (2020).

[21] An example of a micro-cryocooler of this type would be Ricor Inc., model K562S, which weighs 470 grams, consumes 7.5 Watts in steady state, and has cooling power of 0.5 W at 77 K.

[22] M. R. Presland, J. L. Tallon, R. G. Buckley, R. S. Liu, and N. E. Flower, General trends in oxygen stoichiometry effects on T_c in Bi and Tl superconductors, Physica C **176**, 95 (1991).

[23] G. Triscone, J.-Y. Genoud, T. Graf, A. Junod, and J. Muller, Variation of the superconducting properties of $Bi_2Sr_2CaCu_2O_{8+x}$ with oxygen content, Physica C **176**, 247 (1991).[24] L. Y. Hao, M. Ji, J. Yuan, D. Y. An, M. Y. Li, X. J. Zhou, Y. Huang, H. C. Sun, Q. Zhu, F. Rudau, R. Wieland, N. Kinev, J. Li, W.W. Xu, B. B. Jin, J. Chen, T. Hatano, V. P. Koshelets, D. Koelle, R. Kleiner, H. B. Wang, and P. H. Wu, Compact Superconducting Terahertz Source Operating in Liquid Nitrogen, Phys. Rev. Applied **3**, 024006 (2015).

[25] H. Minami, C. Watanabe, T. Kashiwagi, T. Yamamoto, K. Kadowaki, and R. A. Klemm, 0.43 THz emission from high-T_c superconducting emitters optimized at 77 K, J. Phys.: Condensed Matter **28** 025701 (2016).

[26] T. Kitamura, T. Kashiwagi, T. Yamamoto, M. Tsujimoto, C. Watanabe, K. Ishida, S. Sekimoto, K. Asanuma, T. Yasui, K. Nakade, Y. Shibano, Y. Saiwai, H. Minami, R. A. Klemm, and K. Kadowaki, Broadly tunable, high-power terahertz radiation up to 73 K from a stand-alone $Bi_2Sr_2CaCu_2O_{8+\delta}$ mesa, Appl. Phys. Lett **105**, 202603 (2014).

[27] T. Kashiwagi, T. Yamamoto, H. Minami, M. Tsujimoto, R. Yoshizaki, K. Delfanazari, T. Kitamura, C. Watanabe, K. Nakade, T. Yasui, K. Asanuma, Y. Saiwai, Y. Shibano, T. Enomoto, H. Kubo, K. Sakamoto, T. Katsuragawa, B. Marković, J. Mirković, R. A. Klemm, and K. Kadowaki, Efficient Fabrication of Intrinsic-Josephson-Junction Terahertz Oscillators with Greatly Reduced Self-Heating Effects, Phys. Rev. Applied **4**, 054018 (2015).

[28] T. M. Benseman, A. E. Koshelev, K. E. Gray, W.-K. Kwok, U. Welp, K. Kadowaki, M. Tachiki, and T. Yamamoto, Tunable terahertz emission from $Bi_2Sr_2CaCu_2O_{8+\delta}$ mesa devices, Phys. Rev. B **84**, 064523 (2011).

[29] T. Kashiwagi, T. Yuasa, Y. Tanabe, T. Imai, G. Kuwano, R. Ota, K. Nakamura, Y. Ono, Y. Kaneko, M. Tsujimoto, H. Minami, T. Yamamoto, R. A. Klemm, and K. Kadowaki, Improved excitation mode selectivity of high-temperature superconducting terahertz emitters, J. Appl. Phys. **124**, 033901 (2018).

[30] W. C. Stewart, Current-Voltage characteristics of Josephson junctions, Appl. Phys. Lett. **12**, 277 (1968).

[31] T. M. Benseman, A. E. Koshelev, V. Vlasko-Vlasov, Y. Hao, W.-K. Kwok, U. Welp, C. Keiser, B. Gross, M. Lange, D. Koelle, R. Kleiner, H. Minami, C. Watanabe, and K. Kadowaki, Current Filamentation in Large $Bi_2Sr_2CaCu_2O_{8+\delta}$ Mesa Devices Observed via Luminescent and Scanning Laser Thermal Microscopy, Phys. Rev. Applied **3**, 044017 (2015).

[32] K. Delfanazari, H. Asai, M. Tsujimoto, T. Kashiwagi, T. Kitamura, T. Yamamoto, M. Sawamura, K. Ishida, C. Watanabe, S. Sekimoto, H. Minami, M. Tachiki, R. A. Klemm, T. Hattori, and K. Kadowaki, Optics Express, Volume **21**, No. 2 / 2171 (2013).

[33] K. Krishana, N. P. Ong, Q. Li, G. D. Gu, and N. Koshizuka, Science **277**, 83 (1997).

[34] A. Yurgens, Temperature distribution in a large $Bi_2Sr_2CaCu_2O_{8+\delta}$ mesa, Phys. Rev. B **83**, 184501 (2011).

[35] D. G. Cahill and R. O. Pohl, Thermal conductivity of amorphous solids above the plateau, Phys. Rev. B **35**, 4067 (1987).

[36] M. Tsujimoto, T. Doi, G. Kuwano, A. Elarabi, and I. Kakeya, Engineering and characterization of a packaged high-T_c superconducting terahertz source module, Superconductor Science and Technology **30**, 064001 (2017).

[37] Manufacturer's Data Sheet for Stycast 2850FT, Available from Ellsworth Adhesives, W129 N10825 Washington Drive, Germantown, WI 53022.

[38] J. A. King, Material Handbook for Hybrid Microelectronics, Artec House, Norwood MA, 1988.

[39] H. Minami, I. Kakeya, H. Yamaguchi, T. Yamamoto, and K. Kadowaki, Characteristics of terahertz radiation emitted from the intrinsic Josephson junctions in high-T_c superconductor $Bi_2Sr_2CaCu_2O_{8+\delta}$, Appl. Phys. Lett. **95**, 232511 (2009).

[40] R. Cattaneo, E. A. Borodianskyi, A. A. Kalenyuk, and V. M. Krasnov, Superconducting Terahertz Sources with 12% Power Efficiency, Phys. Rev. Applied **16**, L061001 (2021).

[41] V. M. Krasnov, T. Bauch, and P. Delsing, Probing the intrinsic Josephson coupling potential in $Bi_2Sr_2CaCu_2O_{8+\delta}$_superconductors by thermal activation, Phys. Rev. B **72**, 012512 (2005).

[42] H. B. Wang, M. Y. Li, J. Yuan, N. Kinev, J. Li, B. Gross, S. Guenon, A. Ishii, T. Hatano, D. Koelle, R. Kleiner, V. P. Koshelets, and P. H. Wu, A Tunable 350–780 GHz CW solid state oscillator of intrinsic Josephson junctions in a high-Tc superconductor, Proc. 37th Int. Conf. on Infrared, Millimeter, and Terahertz Waves (IEEE, 2012).

[43] H. B. Wang, S. Guenon, J. Yuan, A. Iishi, S. Arisawa, T. Hatano, T. Yamashita, D. Koelle, and R. Kleiner, Hot Spots and Waves in $Bi_2Sr_2CaCu_2O_8$ Intrinsic Josephson Junction Stacks: A Study by Low Temperature Scanning Laser Microscopy, Phys. Rev. Lett. **102**, 017006 (2009).

[44] H. B. Wang, S. Guenon, B. Gross, J. Yuan, Z. G. Jiang, Y. Y. Zhong, M. Grünzweig, A. Iishi, P. H. Wu, T. Hatano, D. Koelle, and R. Kleiner, Coherent Terahertz Emission of Intrinsic Josephson Junction Stacks in the Hot Spot Regime, Phys. Rev. Lett. **105**, 057002 (2010).

[45] T. M. Benseman, A. E. Koshelev, V. Vlasko-Vlasov, Y. Hao, W.-K. Kwok, U. Welp, C. Keiser, B. Gross, M. Lange, D. Kölle, R. Kleiner, H. Minami, C. Watanabe, and K. Kadowaki, Current Filamentation in Large $Bi_2Sr_2CaCu_2O_{8+\delta}$ Mesa Devices Observed via Luminescent and Scanning Laser Thermal Microscopy, Phys. Rev. Applied **3**, 044017 (2015).

[46] K. Kadowaki, M. Tsujimoto, K. Delfanazari, T. Kitamura, M. Sawamura, H. Asai, T. Yamamoto, K. Ishida, C. Watanabe, S. Sekimoto, K. Nakade, T. Yasui, K. Asanuma, T. Kashiwagi, H. Minami, M. Tachiki, T. Hattori, and R. A. Klemm, Quantum terahertz electronics (QTE) using coherent radiation from high temperature superconducting $Bi_2Sr_2CaCu_2O_{8+\delta}$ intrinsic Josephson junctions, Physica C **491**, 2 – 6 (2013).

[47] H. Zhang, R. Wieland, W. Chen, O. Kizilaslan, S. Ishida, C. Han, W. Tian, Z. Xu, Z. Qi, T. Qing, Y.angyang Lu, X. Zhou,N. Kinev, A. B. Ermakov, E. Dorsch, M. Ziegele, D. Koelle, H. Eisaki, Y. Yoshida, V. P. Koshelets, R. Kleiner, H. B. Wang, and P. Wu, Phys. Rev. Appl. **11**, 044004 (2019).

[48] W. Anukool, S. Barakat, C. Panagopoulos, and J. R. Cooper, Effect of hole doping on the London penetration depth in $Bi_{2.15}Sr_{1.85}CaCu_2O_{8+\delta}$ and $Bi_{2.1}Sr_{1.9}Ca_{0.85}Y_{0.15}Cu_2O_{8+\delta}$, Phys. Rev. B **80**, 024516 (2009).

[49] J. W. C. de Vries, Resistivity of thin Au-films as a function of grain diameter and temperature, J. Phys. F: Met. Phys. **17**, 1945 (1987).

[50] J. W. C. de Vries, Temperature and thickness dependence of the resistivity of thin polycrystalline Aluminium, Cobalt, Nickel, Palladium and Gold Films, Thin Solid Films **167**, 25 (1988).

[51] T. H. Gilani, D. Rabchuk, Electrical resistivity of gold thin film as a function of film thickness, Can. J. Phys. **96**, 272 (2018).

[52] D. Y. An, J. Yuan, N. Kinev, M. Y. Li, Y. Huang, M. Ji, H. Zhang, Z. L. Sun, L. Kang, B. B. Jin, J. Chen, J. Li, B. Gross, A. Ishii, K. Hirata, T. Hatano, V. P. Koshelets, D. Koelle, R. Kleiner, H. B. Wang, W. W. Xu, and P. H. Wu, Terahertz emission and detection both based on high-T_c superconductors: Towards an integrated receiver, Applied Physics Letters **102**, 092601 (2013).

[53] S.-Z. Lin and A. E. Koshelev, Synchronization of Josephson oscillations in a mesa array of $Bi_2Sr_2CaCu_2O_{8+\delta}$ through the Josephson plasma waves in the base crystal, Physica C **491**, 24–29 (2013).

[54] A. E. Koshelev and L. N. Bulaevskii, Resonant electromagnetic emission from intrinsic Josephson-junction stacks with laterally modulated Josephson critical current, Phys. Rev. B **77**, 014530 (2008).

Table I

n	m_x	m_y	$f_{n,\ m_x,\ m_y}$	Comment
0	0	3	0.354 THz	Not observed due to retrapping
0	2	0	0.393 THz	Not observed due to retrapping
0	0	4	0.471 THz	Strong emission seen with narrow linewidth from 74 K to 78 K
0	0	5	0.589 THz	These two degenerate modes give strong emission, but with a broad and multipeaked emission spectrum, from 68 K to 75 K
0	3	0	0.589 THz	
0	3	3	0.687 THz	Emission observed with broad and multipeaked emission spectrum, from 65 K to 75 K
0	4	0	0.786 THz	Emission observed with comparatively weak intensity but narrow linewidth, from 60 K to 64 K

Resonant frequencies given by Equations 1 and 2, calculated for modes of the 300 × 180 × 0.92 μm^3 mesa that might be anticipated to radiate significant amounts of THz power. Frequencies are calculated assuming mode index n = 0, and a far-infrared refractive index of 4.24. Figure 7 shows the temperature dependences of the emission power for several modes.

Figure Captions

Figure 1 (Color online only)

(a) Schematic showing the geometry of a typical Bi-2212 mesa designed for coherent THz emission, after [28], with the IJJ stack having width *w* and total thickness *t*. For clarity, vertical scale is shown greatly exaggerated with respect to lateral scale. Red wavy lines are a schematic indication of the direction of greatest far-field radiated THz intensity, and the indicated wavelength is not drawn to scale. Actual wavelength of the emitted radiation is approximately 600 microns, which is twice the mesa length. Polar angle θ and azimuthal angle ϕ as defined in this work are indicated. Current is supplied to the stacked IJJs via the gold top electrode and sunk via the base crystal. Any DC power dissipated in the device is heatsunk via the base crystal also.

(b) Schematic showing vertical cross-section of the devices studied in this work, including the metal thin films deposited on to the top and bottom surfaces of the Bi-2212 crystal. For clarity, vertical distances are shown greatly exaggerated and not to scale.

(c) Optical micrograph of the four devices studied in this work, with important parts of microchip labeled. Note that the Bi-2212 base crystal is so thin that it is almost transparent, and the metal adhesion layers underneath can be seen. The gold tracks at the bottom end of the mesas are for supplying bias current to the mesas themselves, while those at the top end are current leads for future installation of NiCr thin film heaters, intended for studying the effects of localized heating of the mesas. Note that the metal tracks deposited on the epoxy appear slightly out-of-focus in this image, since the epoxy surface lies a few microns above the plane of the top of the mesas.

Figure 2 (Color online only)

$Q_{IJJ}(T)$ as calculated using Equation 5 for optimally-doped Bi-2212, with p = 0.16 holes per Cu. The experimental datasets obtained from reference [31] only extended as low as 10 Kelvin, so data below this temperature is a linear extrapolation (shown dotted).

Figure 3 (Color online only)

$p = 0.16$, $N = 596$, $300 \times 180 \times 0.92$ microns $(l \times w \times t)$.

(a) Mesa bias current for $300 \times 180 \times 0.92$ μm^3 mesa and total integrated radiated THz power, plotted against mesa bias voltage, at a bath temperature of 77.4 K. Black arrows indicate the direction in which current was swept.

(b) Detail of the THz power emission plotted in (a), close to the emission mode.

(c) Detail of the I-V characteristic plotted in (a), over the same range of voltages as in (b). The dashed black line is a straight line fit through the origin assuming a constant device resistance, allowing us to estimate the excess current and power drawn by the resonant THz mode. The voltage steps labelled with the arrows and red asterisks are discussed in the text.

(d) Main: FTIR spectrum for THz emission from the same device, collected close to maximum emission power at this temperature, labelled as point (i) in Figure 3c. Bias current of 65.4 mA is indicated by the dotted horizontal line in (a) above. As-measured FWHM linewidth is limited by the 2.25 GHz resolution of the spectrometer. Inset: Emission spectrum measured at 61.6 mA on the re-entrant section of the current-voltage curve at the same temperature, labelled as point (ii) in Figure 3c. The emission spectrum is much broader and multimodal, while emission power is much weaker than in the main plot. (Please note the different scales for the power and frequency axes in the inset.)

Figure 4 (Color online only)

$p = 0.16$, $N = 596$, $300 \times 180 \times 0.92$ microns $(l \times w \times t)$.

(a) Current-Voltage characteristics for $300 \times 180 \times 0.92$ μm^3 mesa at a range of cryogenic bath temperatures, showing hysteretic switching of stacked IJJs. For this device, THz emission always occurs on the downward sweep, and only in the low-current bias regime (i.e. not in the backbending regions.)

(b) Total integrated radiated THz power plotted against voltage, for the same device. For clarity, successive curves have been offset by 50 microwatts, and only data recorded on the current downsweep is shown. Note also that the voltage scale differs from that shown in (a). (No THz emission occurs at mesa bias voltages exceeding 1.8 V for this device.)

Figure 5 (1.5-column figure, Color online only)

$p = 0.16$, $N = 596$, $300 \times 180 \times 0.92$ microns $(l \times w \times t)$.

Total integrated radiated THz power for $300 \times 180 \times 0.92$ μm^3 mesa plotted against voltage. This data is for the same device as shown in Figure 4, but at more closely-spaced temperatures. For clarity, successive curves have been offset by 100 microwatts. Vertical dashed lines show the four strongest modes of THz emission, labelled with their most probable indices for (m_x, m_y), assuming $n = 0$.

Figure 6 (Color online only)

$p = 0.16$, $N = 596$, $300 \times 180 \times 0.92$ microns ($l \times w \times t$).

(a) THz emission spectrum as measured by FTIR from $300 \times 180 \times 0.92$ μm^3 mesa, at a cryogenic bath temperature of 70 Kelvin, and a bias current of 58.7 mA. This spectrum is very broad and multipeaked, indicating that synchronization of the junctions is quite unstable under these conditions. The most probable modes being excited are $(n = 0,\ m_x = 3,\ m_y = 0)$ and/or $(n = 0,\ m_x = 0,\ m_y = 5)$.

(b) Angle dependence of the THz emission for this device as measured under the same operating conditions as in (a), as a function of polar angle θ, i.e. when rotating about the long axis of the mesa. For comparison, data from one of the $300 \times 60 \times 0.92$ μm^3 mesas on the same chip is plotted, also when operating at 70 K, in either the $(n = 0,\ m_x = 1,\ m_y = 0)$ mode, and/or the $(n = 0,\ m_x = 0,\ m_y = 5)$ mode. Diagram shows the definition of the polar angle θ and azimuthal angle ϕ as referred to in this work.

Figure 7 (Color online only)

(a) $p = 0.16$, $N = 596$, $300 \times 180 \times 0.92$ microns ($l \times w \times t$). Maximum total radiated THz power that could be generated by the $300 \times 180 \times 0.92$ μm^3 mesa at each temperature (red curve, squares). Where one or more modes could be clearly identified at each temperature, the emission power from each of these is plotted also (diamonds).

(b) Maximum total radiated THz power plotted against temperature, for all four devices fabricated on this chip. Blue curves (circles and triangles) show emission for the two individual $300 \times 60 \times 0.92$ μm^3 mesas. Red curve (squares) shows emission for $300 \times 180 \times 0.92$ μm^3 mesa, while the green dashed curve (inverted triangles) shows emission for the set of three conjoined $300 \times 60 \times 0.92$ μm^3 mesas.

Figure 8 (Color online only)

$p = 0.16$, $N = 596$, $300 \times 180 \times 0.92$ microns ($l \times w \times t$).

(a) Plot of the unusual voltage jumps (labelled with red asterisks) seen for the $300 \times 180 \times 0.92$ μm^3 mesa at a cryogenic bath temperature of 77.4 K. Blue inverted triangles are current-voltage data collected while sweeping the current downwards, while red triangles are current upsweep data. Ten sets of data are plotted sweeping in each direction. Green label (i) indicates the current-voltage point at which the FTIR spectrum shown in Figure 4d was measured. Diagonal dashed black line indicates the tangent to the current-voltage curve, corresponding to the estimated low-bias resistance of the mesa. Vertical dotted line indicates the estimated current-voltage anomaly associated with this THz mode.

(b) Total integrated THz emission power measured while sweeping the current downwards, plotted as a function of bias voltage over the same range as for (a). Data for five downward current sweeps are shown.

(c) THz emission power measured while sweeping the current downwards, plotted as a function of bias current over approximately the equivalent biasing range. Due to the excellent reproducibility of our results with respect to bias current, the five datasets plotted are almost indistinguishable.

Figures

Figure 1 (Color online only)

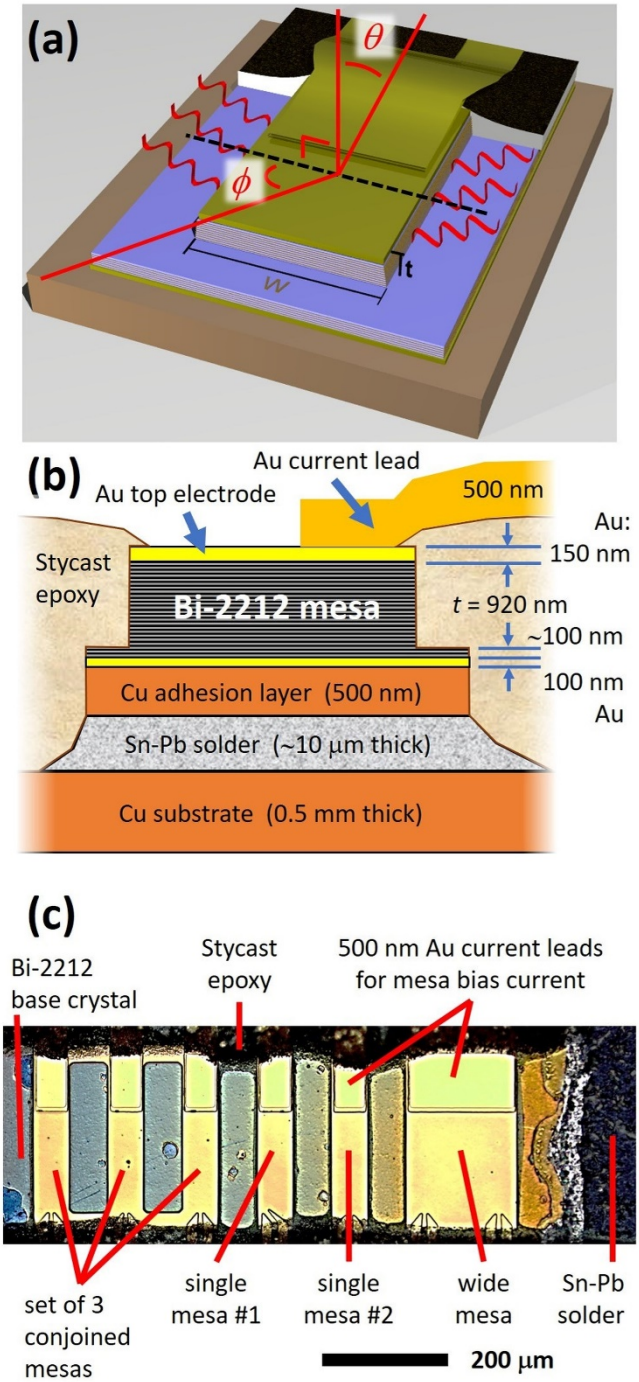

Figure 2 (Color online only)

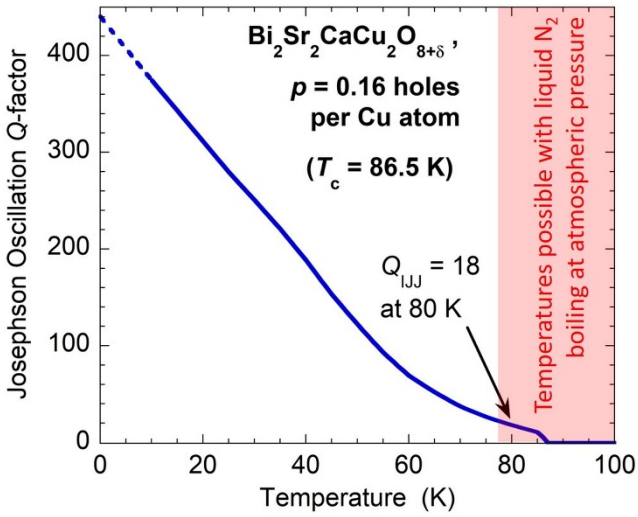

Figure 3 (Color online only)

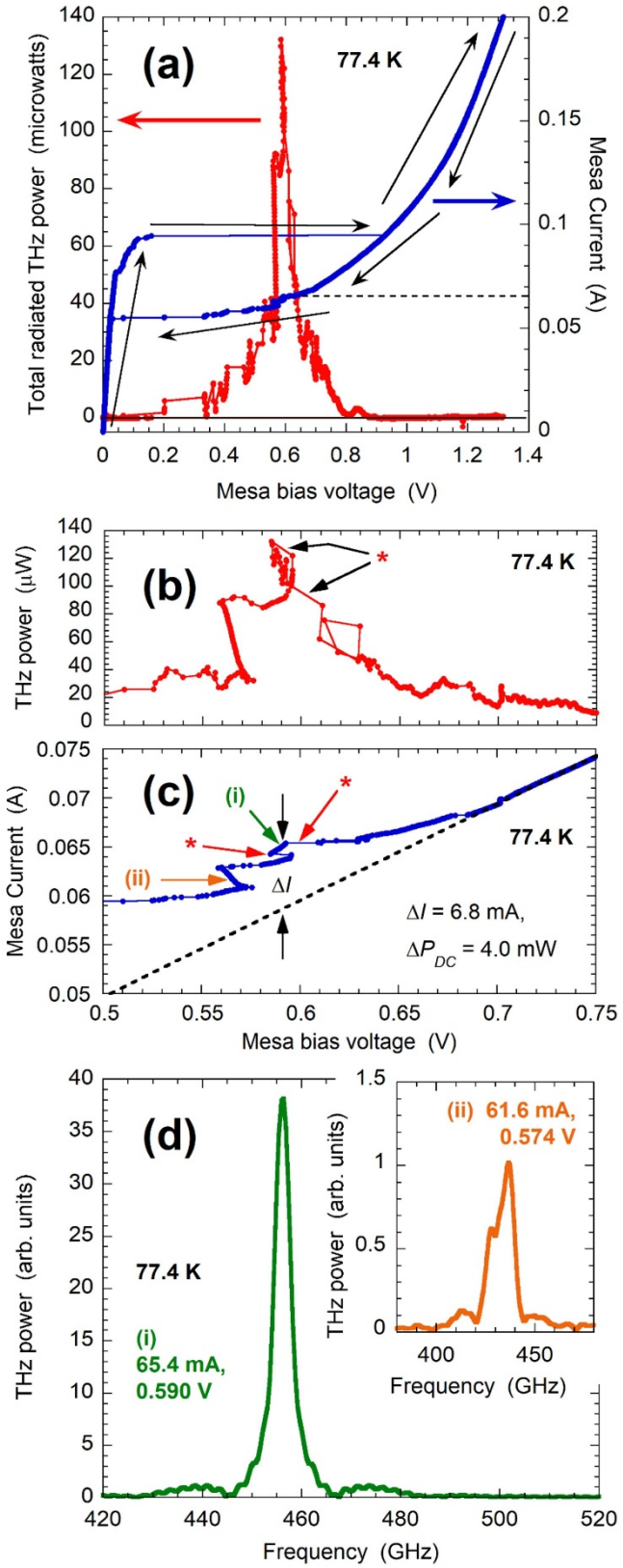

Figure 4 (Color online only)

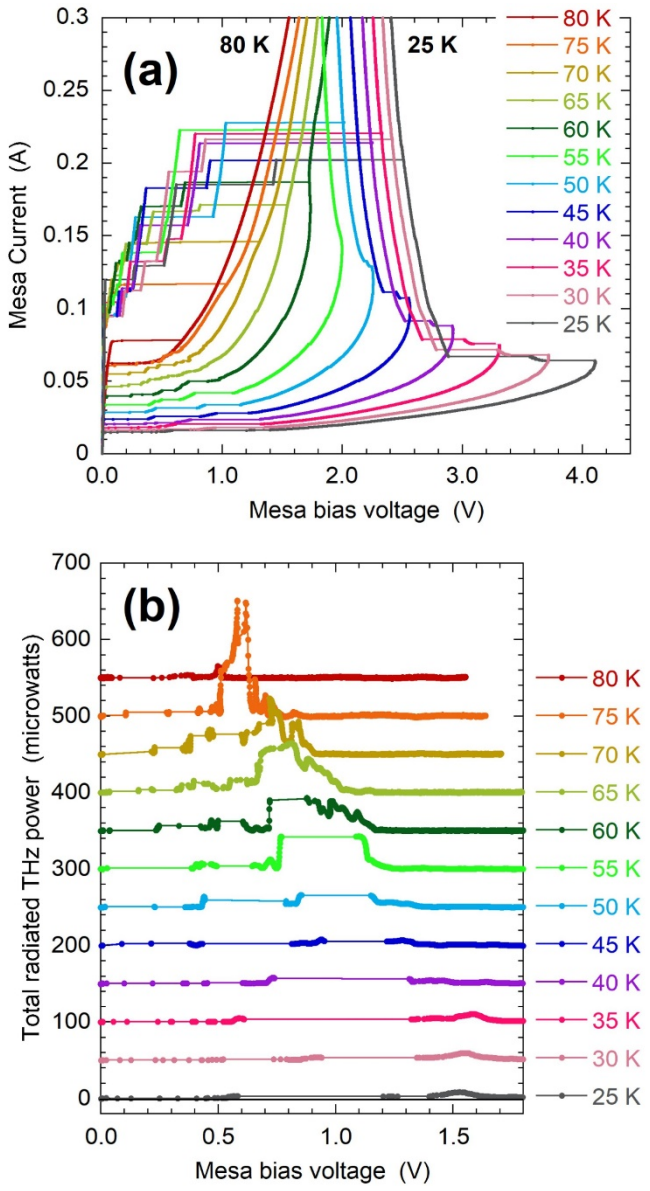

Figure 5 (1.5-column figure, Color online only)

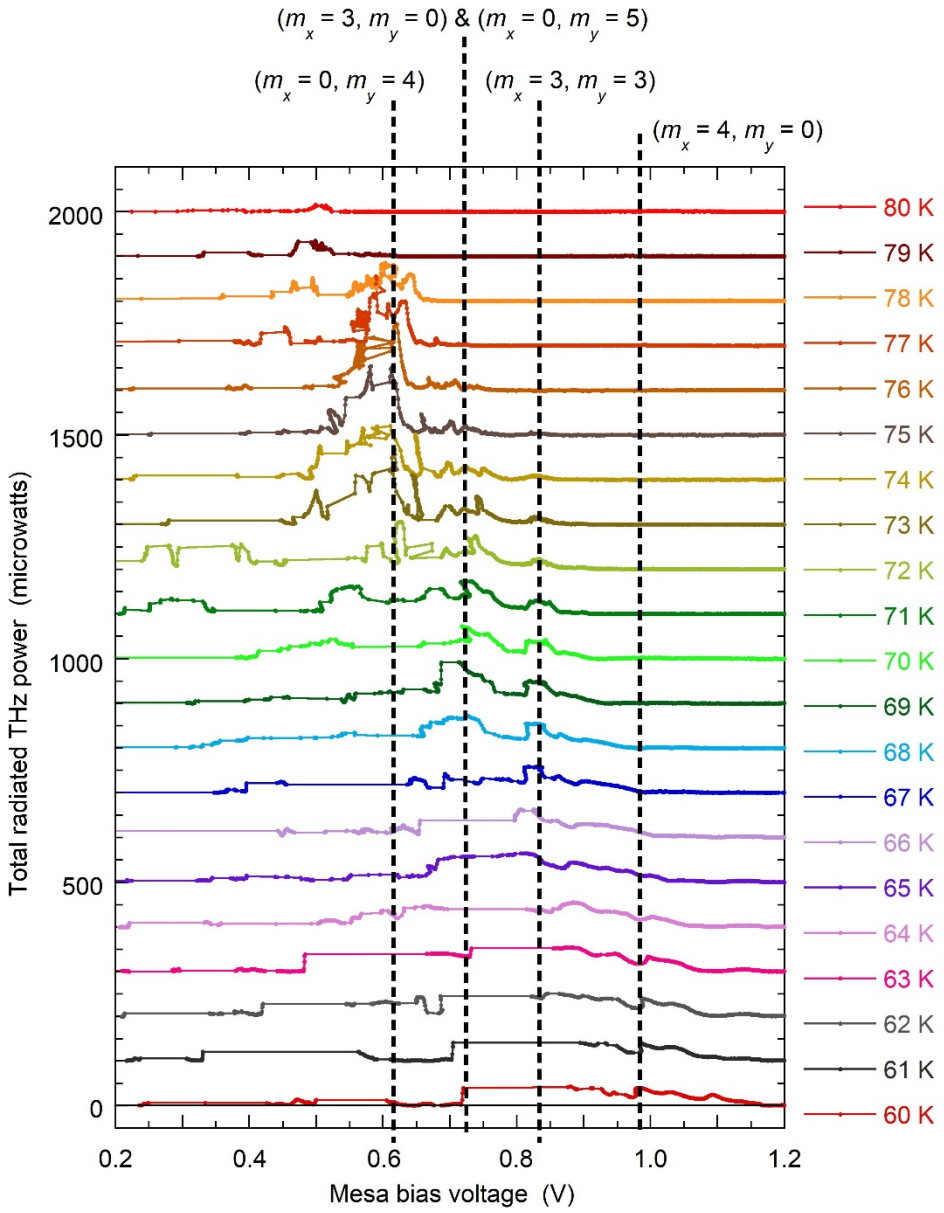

Figure 6 (Color online only)

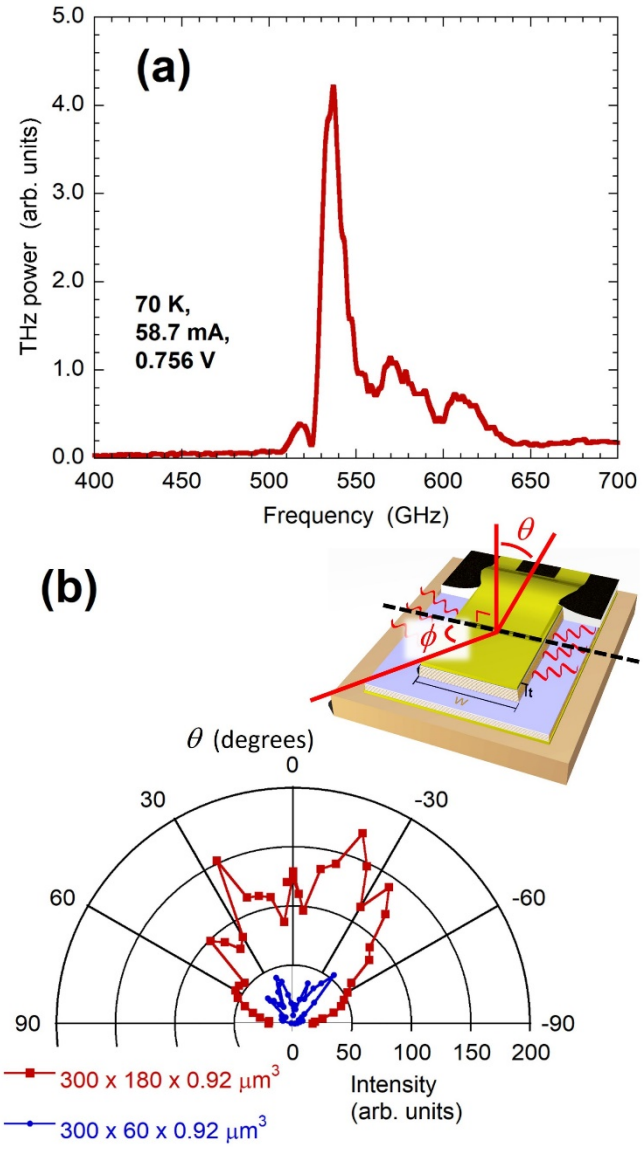

Figure 7 (Color online only)

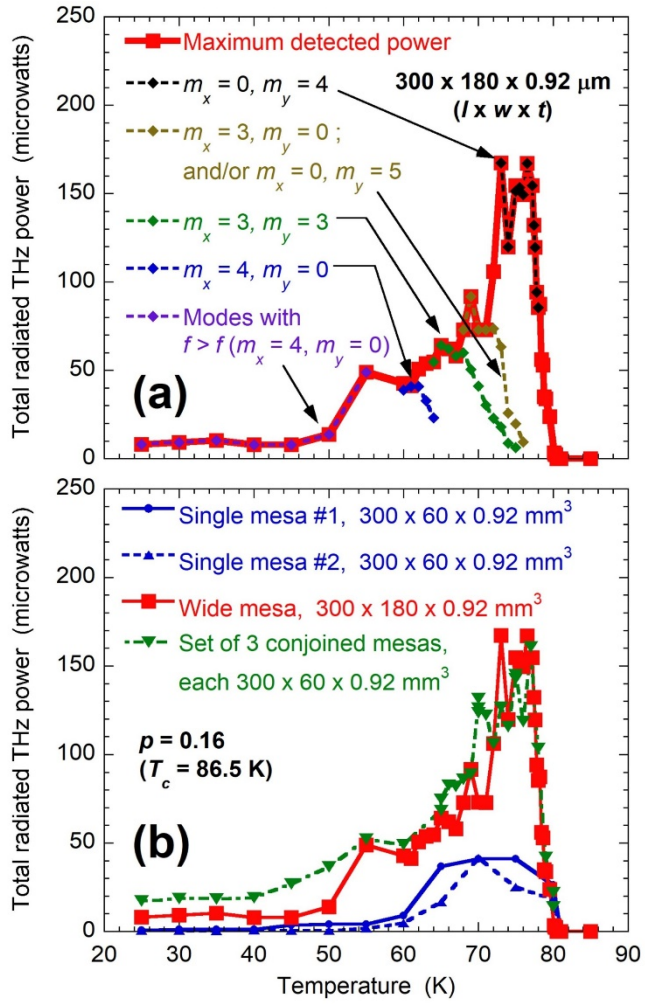

Figure 8 (Color online only)